LETTER

doi:10.1038/nature11312

Activation of specific interneurons improves V1 feature selectivity and visual perception

Seung-Hee Lee[1,2], Alex C. Kwan[1], Siyu Zhang[1], Victoria Phoumthipphavong[1], John G. Flannery[1], Sotiris C. Masmanidis[3], Hiroki Taniguchi[4], Z. Josh Huang[4], Feng Zhang[5], Edward S. Boyden[6], Karl Deisseroth[5] & Yang Dan[1,2]

Inhibitory interneurons are essential components of the neural circuits underlying various brain functions. In the neocortex, a large diversity of GABA (γ-aminobutyric acid) interneurons has been identified on the basis of their morphology, molecular markers, biophysical properties and innervation pattern[1–3]. However, how the activity of each subtype of interneurons contributes to sensory processing remains unclear. Here we show that optogenetic activation of parvalbumin-positive (PV^+) interneurons in the mouse primary visual cortex (V1) sharpens neuronal feature selectivity and improves perceptual discrimination. Using multichannel recording with silicon probes[4,5] and channelrhodopsin-2 (ChR2)-mediated optical activation[6], we found that increased spiking of PV^+ interneurons markedly sharpened orientation tuning and enhanced direction selectivity of nearby neurons. These effects were caused by the activation of inhibitory neurons rather than a decreased spiking of excitatory neurons, as archaerhodopsin-3 (Arch)-mediated optical silencing[7] of calcium/calmodulin-dependent protein kinase IIα (CAMKIIα)-positive excitatory neurons caused no significant change in V1 stimulus selectivity. Moreover, the improved selectivity specifically required PV^+ neuron activation, as activating somatostatin or vasointestinal peptide interneurons had no significant effect. Notably, PV^+ neuron activation in awake mice caused a significant improvement in their orientation discrimination, mirroring the sharpened V1 orientation tuning. Together, these results provide the first demonstration that visual coding and perception can be improved by increased spiking of a specific subtype of cortical inhibitory interneurons.

To allow specific activation of PV^+ interneurons, we injected a Cre-inducible adeno-associated virus (AAV) vector containing the ChR2 gene fused in-frame with the coding sequence for enhanced yellow fluorescent protein (eYFP; Supplementary Fig. 1a)[8] into the V1 of a knock-in mouse line expressing Cre recombinase under the PV promoter (PV-ChR2; see Methods)[9,10]. Three weeks after injection, immunostaining confirmed eYFP expression specific to PV^+ neurons (Fig. 1a). To measure the effect of ChR2 activation, we inserted a multichannel silicon probe[4,5] near to the injection site for simultaneous recording from all cortical layers (Supplementary Fig. 1b). After stimulation with blue (473 nm) laser, a small fraction (12 out of 96; 13%) of the neurons showed significant increases in spontaneous firing rate, whereas 43% (41 out of 96) showed significant decreases (Fig. 1b, c and

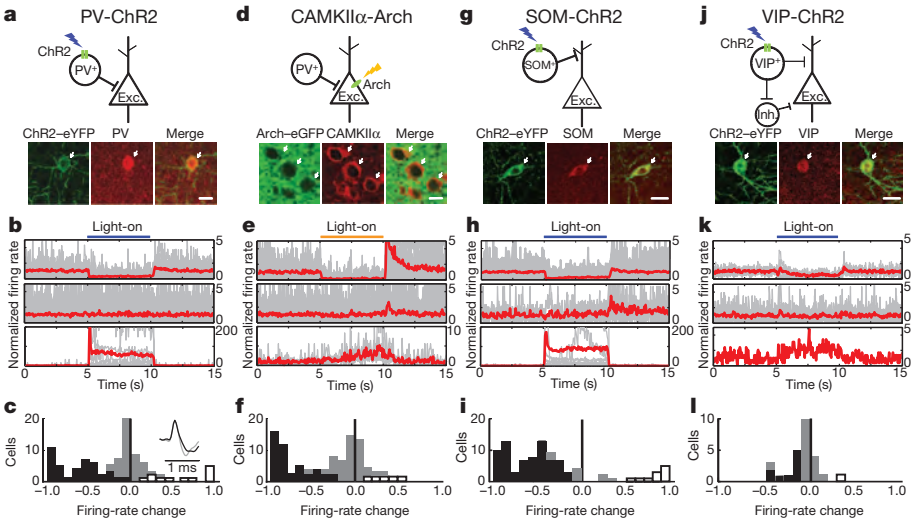

Figure 1 | Optogenetic activation of PV^+, SOM^+ and VIP^+ neurons and silencing of $CAMKII\alpha^+$ neurons. **a**, Fluorescence images of immunostained PV^+ cells (red) expressing ChR2–eYFP (green). Top, schematic illustration of experiment in **a**–**c**. **b**, Peristimulus time histograms of neurons during 30 repeats of blue-laser stimulation. Top, cells showing a significant firing-rate decrease ($P < 0.01$, bootstrap; $n = 41$); middle, cells without significant change ($n = 43$); bottom, cells with a significant increase ($n = 12$). Grey denotes individual cells and red denotes the average within each group. Blue bar indicates the duration of laser stimulation (5 s). The firing rate of each cell was normalized to its mean rate over the 5 s before stimulation. **c**, Histogram of firing-rate changes. Black, grey and white bars represent cells showing significant decreases ($P < 0.01$), no change and significant increases, respectively. Inset, spike waveform averaged across cells with significantly decreased (black) or increased (grey) firing. **d**–**f**, Similar to **a**–**c** for Arch-mediated silencing of $CAMKII\alpha^+$ neurons. **g**–**i**, Similar to **a**–**c** for ChR2-mediated activation of SOM^+ neurons. **j**–**l**, Similar to **a**–**c** for ChR2-mediated activation of VIP^+ neurons. Exc., excitatory neuron; Inh., inhibitory neuron. Thunderbolt marks denote laser stimulation. Scale bars, 15 μm.

[1]Division of Neurobiology, Department of Molecular and Cell Biology, Helen Wills Neuroscience Institute, University of California, Berkeley, California 94720, USA. [2]Howard Hughes Medical Institute, University of California, Berkeley, California 94720, USA. [3]Broad Fellows Program in Brain Circuitry, Kavli Nanoscience Institute, California Institute of Technology, Pasadena, California 91125, USA. [4]Cold Spring Harbor Laboratory, Cold Spring Harbor, New York 11724, USA. [5]Department of Bioengineering, Howard Hughes Medical Institute, Stanford University, Stanford, California 94305, USA. [6]Media Laboratory, Biological Engineering, Brain and Cognitive Sciences, and McGovern Institute, Massachusetts Institute of Technology, Cambridge, Massachusetts 02139, USA.

Supplementary Fig. 1c). The cells with increased firing showed narrower spike waveforms than those with decreased firing (Fig. 1c, inset; peak–trough width, 0.31 ± 0.12 versus 0.44 ± 0.09 ms; mean $\pm$ s.d.), indicating that the PV^+ interneurons activated directly by laser were mostly fast-spiking cells[11]. The decreased spiking of other neurons is probably caused by increased inhibition from the activated PV^+ neurons.

We then measured orientation tuning and direction selectivity of the neurons using drifting grating stimuli, both with and without ChR2 activation. We found that PV^+ neuron activation caused considerable changes in the tuning of other neurons. In addition to the overall firing-rate decrease, we also observed a marked reduction in orientation tuning width and an increase in direction selectivity (Fig. 2a). To quantify these effects, we fitted each tuning curve with a double-Gaussian function (Supplementary Fig. 2a). For all the well-tuned neurons (the tuning curves of which with and without ChR2 activation were well fitted; see Methods), ChR2 activation caused a significant decrease in tuning bandwidth (σ; $P < 10^{-4}$, paired t-test; Fig. 2b) and an increase in direction selectivity index (DSI; $P = 0.007$; Fig. 2c). However, the preferred orientation (θ_0) remained relatively constant (Fig. 2d). Interestingly, all of the putative PV^+ neurons (Fig. 1c, white bars) showed poor tuning even before laser stimulation, consistent with previous findings[12,13]. Although most of the poorly fitted tuning curves showed low signal-to-noise ratio (Supplementary Fig. 2b, c, examples 1, 2), a few had relatively reliable tuning curves showing several irregular peaks (Supplementary Fig. 2b, c, examples 3–6). Laser stimulation also sharpened the tuning of some of these cells, although the degree of sharpening was not well quantified by curve fitting.

The decrease in σ was correlated with the reduction in firing rate (Supplementary Fig. 3e), suggesting that the enhanced selectivity depends on the increase in inhibition. However, we also wondered whether an overall reduction in cortical firing is sufficient to enhance the selectivity without interneuron activation. As an alternative method to decrease cortical spiking, we expressed the light-activated proton pump Arch[7] in $CAMKII\alpha^+$ excitatory neurons by injecting AAV (Supplementary Fig. 1a) into the V1 of the CAMKIIα-Cre mice[14] (CAMKIIα-Arch; Fig. 1d). Arch-mediated partial silencing of $CAMKII\alpha^+$ neurons caused decreases in the spontaneous (Fig. 1e, f and Supplementary Fig. 1c) and visually evoked (Supplementary Fig. 1c, d) firing rates, similar to PV^+ neuron activation. However, $CAMKII\alpha^+$ neuron silencing caused no significant change in σ ($P = 0.75$; Fig. 2f) or DSI ($P = 0.68$; Fig. 2g). In addition, there was no significant correlation between the firing-rate reduction and change in σ or DSI (Supplementary Fig. 3f, j).

Next, we wanted to test whether the enhanced selectivity required a general increase in inhibition or specific activation of PV^+ interneurons.

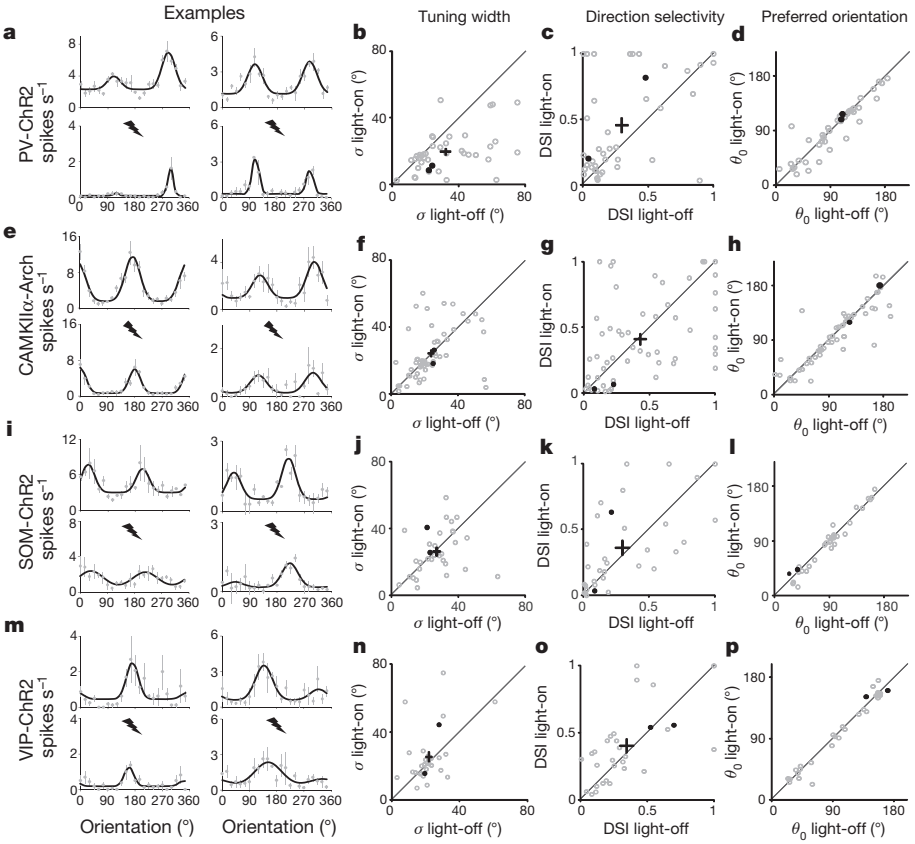

Figure 2 | PV^+ activation enhances V1 stimulus selectivity. **a**, Tuning curves of two cells, each box for one cell. Grey dots denote measured firing rates and black line denotes fitted curve. Top plot depicts no laser; bottom plot depicts laser stimulation. **b**–**d**, Population summary of ChR2-mediated changes in stimulus selectivity ($n = 41$). Each circle represents one cell and cross represents population average. **b**, Tuning width (σ), light-off, $32.1 \pm 2.9°$ and light-on, $19.7 \pm 1.9°$; 22% individual neurons showed a significant decrease at $P < 0.01$ (bootstrap) and none showed a significant increase. **c**, DSI, light-off, 0.30 ± 0.05 and light-on, 0.45 ± 0.06; 11% of neurons showed a significant increase and none showed a significant decrease. **d**, Preferred orientation (θ_0), median difference between light-on and light-off, 6.2°. For neurons in **b**–**d**, the laser reduced visually evoked firing rate from 5.5 ± 0.6 to 2.8 ± 0.5 spikes s^{-1} ($P < 10^{-4}$, paired t-test). Filled circles, example cells in **a**. **e**–**h**, Similar to **a**–**d** for $CAMKII\alpha^+$ silencing. Mean firing rate reduced from 3.0 ± 0.4 to 2.2 ± 0.4 spikes s^{-1} ($n = 56$; $P = 0.003$). **f**, σ, light-off, $23.6 \pm 1.8°$ and light-on, $24.3 \pm 2.0°$. No individual cell showed a significant change. **g**, DSI, light-off, 0.43 ± 0.04 and light-on, 0.41 ± 0.04. **h**, θ_0, median difference, 5.4°. **i**–**l**, Similar to **a**–**d** for SOM-ChR2 mice. Firing rate reduced from 3.4 ± 0.6 to 1.9 ± 0.4 spikes s^{-1} ($P < 10^{-3}$). **j**, σ, light-off, $26.9 \pm 2.1°$ and light-on, $26.2 \pm 2.3°$, $n = 33$. No individual cell showed a significant change. **k**, DSI, light-off, 0.29 ± 0.05 and light-on, 0.36 ± 0.06. **l**, θ_0, median difference, 5.7°. **m**–**p**, Similar to **a**–**d** for VIP-ChR2 mice ($n = 31$). **n**, σ, light-off, $21.8 \pm 1.8°$ and light-on, $25.5 \pm 2.8°$. **o**, DSI, light-off, 0.35 ± 0.05 and light-on, 0.41 ± 0.05. **p**, θ_0, median difference, 5.6°. All data are mean $\pm$ s.e.m.

In addition to PV^+ neurons, somatostatin $(SOM)^+$ and vasointestinal peptide $(VIP)^+$ neurons constitute two other major subtypes of GABAergic interneurons[2]. To test their roles in shaping V1 selectivity, we induced cell-type-specific expression of ChR2–eYFP in SOM-Cre or VIP-Cre mice (Fig. 1g, j). In the SOM-ChR2 mice, the laser also caused increased spiking of a few neurons (11 out of 91) but decreased firing in most of the neurons (71 out of 91) (Fig. 1h, i, and Supplementary Fig. 1c, d). In fact, compared with the PV-ChR2 group, a higher percentage of neurons showed decreased firing. However, SOM^+ activation caused no significant effect on either σ ($P = 0.79$; Fig. 2i, j) or DSI ($P = 0.17$; Fig. 2i, k). In VIP-ChR2 mice, laser stimulation also induced no significant change in σ ($P = 0.16$; Fig. 2m, n) or DSI ($P = 0.16$; Fig. 2m, o), and only a mild change in firing rate (Fig. 1k, l and Supplementary Fig. 1c, d). The change in σ showed a negative correlation with firing-rate change (Supplementary Fig. 3h), opposite to PV^+ activation (Supplementary Fig. 3e). This may be because the VIP^+ neurons also innervate inhibitory interneurons[15], thus causing both inhibition and disinhibition. In addition to σ, tuning measured by orientation selectivity index was also improved by PV^+ activation, but not by $CAMKII\alpha^+$ silencing or SOM^+ or VIP^+ activation (Supplementary Fig. 4).

Even among the PV-ChR2, SOM-ChR2 and CAMKIIα-Arch groups, the degrees of firing-rate suppression were not identical. To ensure that the difference in tuning width reduction was not caused by differences in firing-rate suppression, we selected neurons from each group that showed intermediate levels of suppression (firing-rate change, −0.75 to −0.3; Supplementary Fig. 5a). Although the spike-rate suppression is well matched across groups within this range (mean rate change, −0.51 (PV), −0.50 (SOM), −0.50 (CAMKIIα)), laser stimulation caused a significant decrease in σ in the PV (-0.19 ± 0.05; mean ± s.e.m.) but not the SOM (0.01 ± 0.09) or CAMKIIα (-0.05 ± 0.03) groups. The magnitudes of reduction in σ were significantly different between the PV and SOM or CAMKIIα groups (Supplementary Fig. 5b). We also noticed that neurons in these groups showed different initial tuning widths ($\sigma_{\text{light-off}}$). To ensure that the difference in tuning width reduction was not caused by the difference in $\sigma_{\text{light-off}}$, we selected neurons with $\sigma_{\text{light-off}}$ falling within two ranges: the broad (25–50°) and narrow (0–25°) ranges. Within each range, the median values of $\sigma_{\text{light-off}}$ were not significantly different across groups, but laser stimulation caused a significant decrease in σ in the PV-ChR2 group (broad, -0.28 ± 0.09; narrow, -0.11 ± 0.05) and not in any other group (Supplementary Fig. 5c, d). Furthermore, within each range the amount of decrease in σ was significantly different between the PV group and other groups.

Although the lack of effect of VIP^+ activation on σ is not surprising given its moderate effect on firing rate, what underlies the difference between SOM^+ and PV^+ neurons is not obvious. Tuning of a sensory neuron depends on its firing rate versus input current (F–I) curve: subtractive modulation of the F–I curve causes sharpening of tuning, whereas divisive modulation has no effect[16]. We therefore tested the effects of SOM^+ and PV^+ activation on neuronal F–I functions using *in vivo* whole-cell recording (see Methods). For each neuron we measured firing rate versus injected depolarizing current. We found that PV^+ activation caused a large increase in spiking threshold ($P = 6 \times 10^{-4}$, paired t-test) without significantly changing the slope ($P = 0.34$; Fig. 3a–d), but SOM^+ activation caused a marked reduction of the slope ($P = 0.02$) without a significant change in threshold ($P = 0.18$; Fig. 3e–h). These effects may be related to the different subcellular targeting of PV^+ and SOM^+ neurons onto pyramidal neurons (perisomatic versus dendritic)[17]. When we plotted the median response of each group at each orientation with versus without laser stimulation, we also found a strong subtractive effect of PV^+ activation but a primarily divisive effect of SOM^+ activation (Supplementary Fig. 6).

Changes in V1 orientation tuning can, in principle, affect perceptual discrimination[18,19]. To test the functional consequence of sharpened tuning, we applied laser stimulation to awake PV-ChR2 mice while they performed orientation discrimination. The head-restrained mice were trained on a go/no-go task and rewarded for licking in response to a grating at one of two orientations[20] (see Methods, Fig. 4a, b and Supplementary Movie 1). For an easy discrimination task (difference between go and no-go orientations $\Delta\theta = 90°$), the performance measured by the divergence between hit and false-alarm rates (Fig. 4c) and discriminability (d'; Fig. 4d) improved systematically over days. As expected, d' increased monotonically with $\Delta\theta$ (Fig. 4e). After the performance reached a steady state, we tested the effect of laser and found a significant improvement in d' at a range of $\Delta\theta$ (Fig. 4f and Supplementary Fig. 7a–c). To ensure that the improvement was caused by optical activation of PV^+ neurons rather than through the retinal photoreceptors activated by scattered laser, we performed a control experiment in mice that were not virus-infected and found no significant increase in d' (Fig. 4g). Separate electrophysiological experiments in awake mice showed that PV^+ activation also caused a significant sharpening of tuning ($P < 0.05$; Supplementary Fig. 8), similar to that in anaesthetized mice (Fig. 2a, b). Thus, the sharpening of V1 orientation tuning induced by PV^+ activation can facilitate orientation discrimination. Unlike the learning curve shown in Fig. 4d, in which d' improved steadily over 5–10 days of training, the effect of PV^+ activation showed no systematic change over several

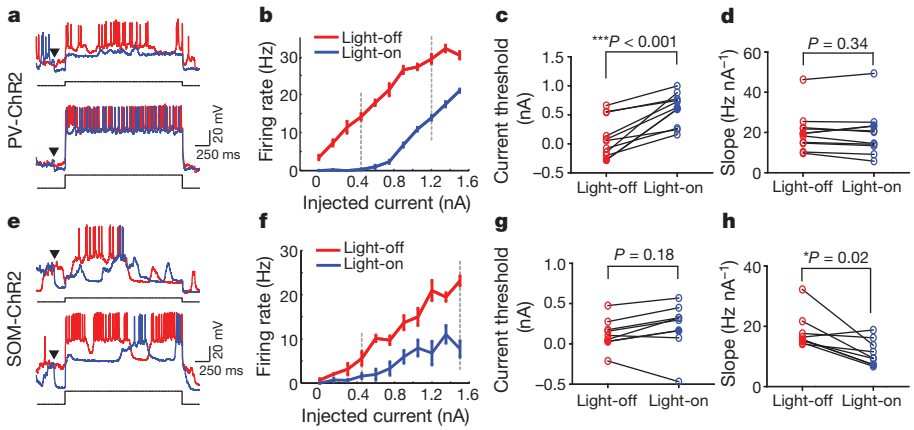

Figure 3 | Effects of PV^+ and SOM^+ activation on F–I function. **a**, Example traces showing neuronal spiking evoked by current injection. Red indicates voltage trace without laser and blue indicates voltage trace with laser. Arrowhead indicates laser onset (laser offset, 800 ms after current injection; not shown). Current amplitude, 0.45 nA (upper) and 1.2 nA (lower). **b**, F–I curve of the cell shown in **a**. Red denotes firing rate without laser and blue denotes firing rate with laser. Dashed lines indicate current amplitudes shown in **a**. **c**, **d**, Summary of threshold (lowest current that evokes spiking) and F–I slope with and without laser. Each symbol represents one cell ($n = 10$). **e**–**h**, Similar to **a**–**d** for SOM^+ activation ($n = 8$). All data are ± s.e.m.

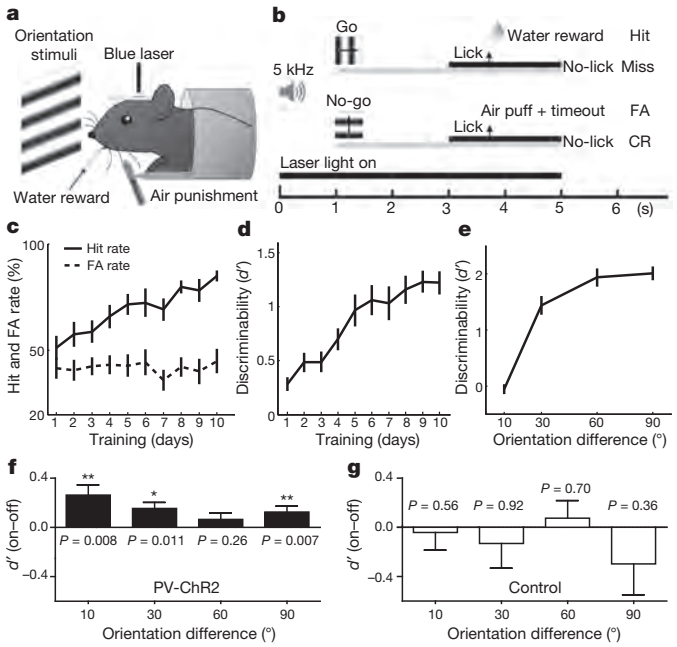

Figure 4 | PV$^+$ activation improves perceptual discrimination. **a**, Schematic of behavioural experiment. **b**, Task design. Grey bar indicates the duration of visual stimulation and black bar indicates the response window. CR, correct rejection; FA, false alarm. **c**, Changes in hit and FA rates of PV-ChR2 mice over the training period ($n = 25$ mice). **d**, Changes in d' over training period. **e**, d' versus $\Delta\theta$. Data in **c**–**e** were collected without laser stimulation. **f**, Laser-induced changes in d' in PV-ChR2 mice, significant at $\Delta\theta = 10^\circ$ ($P = 0.008$, Wilcoxon signed-rank test, 0.032 after Bonferroni correction; $n = 9$ mice), $\Delta\theta = 30^\circ$ ($P = 0.011$; $n = 19$) and $\Delta\theta = 90^\circ$ ($P = 0.007$; $n = 25$). **g**, Similar to **f** but for control mice ($n = 10$). All data are mean ± s.e.m.

days of testing (Supplementary Fig. 7d), suggesting that the effect was not caused by learning of a distorted perception owing to PV$^+$ activation.

Previous pharmacological experiments have shown that the endogenous level of GABAergic inhibition is necessary for orientation tuning and direction selectivity[21,22]. Our study showed that increasing inhibitory neuron activity above the normal level can further sharpen cortical feature selectivity and improve perceptual discrimination. A recent study showed that PV$^+$ activation only moderately affects the tuning of V1 neurons[23]. This is probably caused by the relatively low level of PV$^+$ activation compared with our study, as the increase in stimulus selectivity is strongly correlated with the degree of firing-rate suppression (Supplementary Fig. 3e, i). Interestingly, studies in awake, behaving primates have shown that increases in task difficulty[24] and attention[25] are accompanied by a preferential increase in the firing of fast-spiking neurons, many of which are likely to be PV$^+$ interneurons[11]. This suggests that the level of inhibitory activity can be dynamically regulated by top-down mechanisms to meet changing behavioural demands.

A long-standing debate on the mechanism for orientation tuning is whether the excitatory and inhibitory inputs show similar tuning[26]. In the rodent V1, whether inhibitory interneurons are well tuned has also been controversial[12,13,27]. Our results show that an increase in the untuned activity of inhibitory interneurons is sufficient to sharpen orientation tuning, consistent with previous theoretical prediction[28]. Furthermore, although driving either PV$^+$ or SOM$^+$ interneurons markedly suppressed cortical spiking, only PV$^+$ activation could sharpen orientation tuning. This specificity may be attributable to the powerful perisomatic inhibition exerted by PV$^+$ neurons[1,29]. Recent studies have demonstrated the importance of PV$^+$ neurons in gating developmental plasticity[30] and generating gamma oscillations[9,10]. Our results show that these interneurons also have a unique role in visual coding and perception.

METHODS SUMMARY

AAV was injected into the V1 of adult (P40-60) PV-Cre, CAMKIIα-Cre, SOM-Cre or VIP-Cre mice. For recording and behavioural training in awake mice, the head plate was implanted in the same surgery as the virus injection; recording or training was performed 2–6 weeks after surgery. For ChR2 (Arch) activation, an optic fibre coupled to blue (yellow/green) laser was placed on top of the injection site. For measuring orientation tuning, eight repeats of drifting sinusoidal grating (spatial frequency, 0.04 cycles per degree; temporal frequency, 2 Hz; 100% contrast) were presented in 24 directions (0–360°) in pseudorandom sequence. Blocks of trials with or without laser were interleaved. To quantify tuning, we fitted each tuning curve by double-Gaussian function. To test orientation discrimination, mice were trained to discriminate between go and no-go stimuli (drifting gratings at different orientations) for a water reward[20].

Full Methods and any associated references are available in the online version of the paper.

Received 18 May 2011; accepted 11 June 2012.
Published online 8 August 2012.

1. Markram, H. *et al.* Interneurons of the neocortical inhibitory system. *Nature Rev. Neurosci.* **5,** 793–807 (2004).
2. Xu, X. M., Roby, K. D. & Callaway, E. M. Immunochemical characterization of inhibitory mouse cortical neurons: three chemically distinct classes of inhibitory cells. *J. Comp. Neurol.* **518,** 389–404 (2010).
3. Ascoli, G. A. *et al.* Petilla terminology: nomenclature of features of GABAergic interneurons of the cerebral cortex. *Nature Rev. Neurosci.* **9,** 557–568 (2008).
4. Blanche, T. J., Spacek, M. A., Hetke, J. F. & Swindale, N. V. Polytrodes: high-density silicon electrode arrays for large-scale multiunit recording. *J. Neurophysiol.* **93,** 2987–3000 (2005).
5. Du, J. G. *et al.* High-resolution three-dimensional extracellular recording of neuronal activity with microfabricated electrode arrays. *J. Neurophysiol.* **101,** 1671–1678 (2009).
6. Deisseroth, K. Optogenetics. *Nature Methods* **8,** 26–29 (2011).
7. Chow, B. Y. *et al.* High-performance genetically targetable optical neural silencing by light-driven proton pumps. *Nature* **463,** 98–102 (2010).
8. Zhang, F. *et al.* Optogenetic interrogation of neural circuits: technology for probing mammalian brain structures. *Nature Protocols* **5,** 439–456 (2010).
9. Sohal, V. S., Zhang, F., Yizhar, O. & Deisseroth, K. Parvalbumin neurons and gamma rhythms enhance cortical circuit performance. *Nature* **459,** 698–702 (2009).
10. Cardin, J. A. *et al.* Driving fast-spiking cells induces gamma rhythm and controls sensory responses. *Nature* **459,** 663–667 (2009).
11. Toledo-Rodriguez, M. *et al.* Correlation maps allow neuronal electrical properties to be predicted from single-cell gene expression profiles in rat neocortex. *Cereb. Cortex* **14,** 1310–1327 (2004).
12. Kerlin, A. M., Andermann, M. L., Berezovskii, V. K. & Reid, R. C. Broadly tuned response properties of diverse inhibitory neuron subtypes in mouse visual cortex. *Neuron* **67,** 858–871 (2010).
13. Ma, W. P. *et al.* Visual representations by cortical somatostatin inhibitory neurons–selective but with weak and delayed responses. *J. Neurosci.* **30,** 14371–14379 (2010).
14. Tsien, J. Z. *et al.* Subregion- and cell type-restricted gene knockout in mouse brain. *Cell* **87,** 1317–1326 (1996).
15. Dávid, C., Schleicher, A., Zuschratter, W. & Staiger, J. F. The innervation of parvalbumin-containing interneurons by VIP-immunopositive interneurons in the primary somatosensory cortex of the adult rat. *Eur. J. Neurosci.* **25,** 2329–2340 (2007).
16. Ayaz, A. & Chance, F. S. Gain modulation of neuronal responses by subtractive and divisive mechanisms of inhibition. *J. Neurophysiol.* **101,** 958–968 (2009).
17. Mehaffey, W. H., Doiron, B., Maler, L. & Turner, R. W. Deterministic multiplicative gain control with active dendrites. *J. Neurosci.* **25,** 9968–9977 (2005).
18. Kang, K. J., Shapley, R. M. & Sompolinsky, H. Information tuning of populations of neurons in primary visual cortex. *J. Neurosci.* **24,** 3726–3735 (2004).
19. Schoups, A., Vogels, R., Qian, N. & Orban, G. Practising orientation identification improves orientation coding in V1 neurons. *Nature* **412,** 549–553 (2001).
20. Andermann, M. L. K. e. r. l. i. n. A. M. &. R. e. i. d. R. C. Chronic cellular imaging of mouse visual cortex during operant behavior and passive viewing. *Front. Cell. Neurosci.* **4,** 3 (2010).
21. Sillito, A. M. Effectiveness of bicuculline as an antagonist of GABA and visually evoked inhibition in the cat's striate cortex. *J. Physiol. (Lond.)* **250,** 287–304 (1975).
22. Nelson, S., Toth, L., Sheth, B. & Sur, M. Orientation selectivity of cortical neurons during intracellular blockade of inhibition. *Science* **265,** 774–777 (1994).
23. Atallah, B. V., Bruns, W., Carandini, M. & Scanziani, M. Parvalbumin-expressing interneurons linearly transform cortical responses to visual stimuli. *Neuron* **73,** 159–170 (2012).
24. Chen, Y. *et al.* Task difficulty modulates the activity of specific neuronal populations in primary visual cortex. *Nature Neurosci.* **11,** 974–982 (2008).
25. Mitchell, J. F., Sundberg, K. A. & Reynolds, J. H. Differential attention-dependent response modulation across cell classes in macaque visual area V4. *Neuron* **55,** 131–141 (2007).
26. Ferster, D. & Miller, K. D. Neural mechanisms of orientation selectivity in the visual cortex. *Annu. Rev. Neurosci.* **23,** 441–471 (2000).

27. Runyan, C. A. *et al.* Response features of parvalbumin-expressing interneurons suggest precise roles for subtypes of inhibition in visual cortex. *Neuron* **67,** 847–857 (2010).
28. Troyer, T. W., Krukowski, A. E., Priebe, N. J. & Miller, K. D. Contrast-invariant orientation tuning in cat visual cortex: thalamocortical input tuning and correlation-based intracortical connectivity. *J. Neurosci.* **18,** 5908–5927 (1998).
29. Di Cristo, G. *et al.* Subcellular domain-restricted GABAergic innervation in primary visual cortex in the absence of sensory and thalamic inputs. *Nature Neurosci.* **7,** 1184–1186 (2004).
30. Hensch, T. K. Critical period plasticity in local cortical circuits. *Nature Rev. Neurosci.* **6,** 877–888 (2005).

Supplementary Information is linked to the online version of the paper at www.nature.com/nature.

Acknowledgements We thank M. Goard, L. Pinto, M. Xu and M. Viesel for help with experimental setup, A. Kaluszka for help with data analysis and H. Alitto and M. Poo for discussion and comments on the manuscript. This work was supported by National Institutes of Health grants R01 EY018861 and PN2 EY018241 and National Science Foundation grant 22250400-42533.

Author Contributions S.-H.L. and Y.D. conceived and designed the experiments. S.-H.L. performed and organized all the experiments. A.C.K. developed the head-fixed awake mouse preparation and behavioural task setup. S.Z. performed whole-cell recording experiments. V.P. performed some of the virus injection and head-plate implant surgeries. J.G.F. supported viral vector preparation. S.C.M. manufactured silicon probe (type II). H.T. and Z.J.H. generated SOM-Cre and VIP-Cre mouse lines. E.S.B. generated the Arch–eGFP viral vector. F.Z. and K.D. developed the ChR2–eYFP viral vector. S.-H.L., A.K. and Y.D. analysed the data. S.-H.L. and Y.D. wrote the manuscript. All authors discussed the results and commented on the manuscript.

Author Information Reprints and permissions information is available at www.nature.com/reprints. The authors declare no competing financial interests. Readers are welcome to comment on the online version of this article at www.nature.com/nature. Correspondence and requests for materials should be addressed to Y.D. (ydan@berkeley.edu).

METHODS

AAV vectors. ChR2 fused to eYFP (ChR2–eYFP) and Arch fused to enhanced green fluorescent protein (eGFP) (Arch–eGFP) were cloned into pAAV-MCS (Stratagene) in an antisense direction flanked by a pair of canonical *loxP* sites and a pair of mutated *lox2272* sites. AAV particles (serotype 2) were produced by co-transfection of packaging plasmids into HEK293T cells, and cell lysates were fractionated by iodixanol gradient ultracentrifugation[31]. Viral particles were further purified from the crude fraction by heparin affinity column (HiTrap Heparin HP Columns; GE Healthcare), desalted and concentrated with Amicon Ultra Centrifugal Filter (100K, Millipore) (1×10^{12}–1×10^{14} particles ml^{-1} in PBS buffer). AAV serotype 2/2 was used for ChR2 and serotypes 2/2 and 2/8 were used for Arch. All recombinant viral vectors were cloned in the genomic DNA backbone of AAV serotype 2, and we generated the hybrid serotype using different capsids from the corresponding serotypes.

Virus injection and head-plate implant. All experimental procedures were approved by the Animal Care and Use Committee at the University of California, Berkeley. For virus injection, young adult (postnatal day (P)40–P60, body weight: 20–30 g) PV-Cre (Jackson Laboratory), CAMKIIα-Cre (Jackson Laboratory), SOM-Cre (Cold Spring Harbor Laboratory) or VIP-Cre (Cold Spring Harbor Laboratory) mice were anaesthetized with ketamine (intraperitoneally; 70 mg per kg body weight) and supplemented with 1.5% isoflurane and 1.5% oxygen. A craniotomy (~0.5 mm diameter) was made above the monocular region of the right V1 (3.7–3.8 mm posterior to bregma, 2 mm lateral from midline), and 1 μl of AAV (containing $>1\times10^{9}$ viral particles) was injected into the cortex at a depth of 250–500 μm. For recording and behavioural training in awake mice, custom-designed head plates were implanted straight after the virus injection. Small screws (Small Parts) and dental acrylic (Diamond Springs) were used to fix the head plate onto the skull. The skull over the virus-injected area was covered by a silicon sealant (Kwik-Cast, WPI).

Immunohistochemistry. Two weeks after the virus injection, the mice were deeply anaesthetized with isoflurane and immediately perfused with chilled 0.1 M PBS followed by 4% paraformaldehyde (w/v) in PBS. The brain was removed and post-fixed for 15 h at 4 °C. After fixation, the brain was placed in 30% sucrose (w/v) in PBS solution overnight at 4 °C. After embedding and freezing, the brain was sectioned into 40 μm coronal slices using a cryostat (Thermo Fisher). Slices were incubated with blocking solution (2% normal goat serum in PBS with 0.5% Triton X-100) for 2 h at 20 °C and then with primary antibodies diluted in blocking solution overnight at 4 °C. The following primary antibodies were used: anti-PV primary antibody (PVG-214, Swant; 1:1,000), anti-SOM antibody (MAB353, Millipore/Chemicon; 1:200), anti-VIP antibody (20077, ImmunoStar; 1:500) or anti-CAMKIIα antibody (sc-13141, Santa Cruz Biotechnology; 1:50). Slices were then washed three times with the blocking solution and incubated with the secondary antibody for 2 h at 20 °C (for PV and VIP, Alexa594-conjugated anti-rabbit IgG, Invitrogen, 1:1,000; for CAMKIIα, Alexa568-conjugated anti-mouse IgG, Invitrogen, 1:200 and for SOM, Cy3-conjugated anti-rat IgG, Jackson ImmunoResearch, 1:200). Slices were washed three times with PBS (10 min each) and mounted with 4′,6-diamidino-2-phenylindole (DAPI)-containing Vectashield (Vector Laboratories). Fluorescence images were taken under a confocal microscope (Zeiss).

Electrophysiology. Recording experiments were performed 2–6 weeks after virus injection. For anaesthetized experiments, mice were anaesthetized with urethane (intraperitoneally, 1.65 g per kg body weight) supplemented with 1–1.5% isoflurane and restrained in a stereotaxic apparatus (David Kopf Instruments). Body temperature was maintained at 37.5 °C through a heating pad (Harvard Apparatus). For recording in awake mice, the body of the mouse was placed in an acrylic tube (2.9 cm inner diameter; McMaster) and the head plate was fixed on a holder attached to the air table. The mouse could move its body inside the tube while the head was fixed. While the animal was under gas anaesthesia (1.5% isoflurane in oxygen), a craniotomy (~1 mm diameter) was made again above the virus-injected area and a small portion of the dura was removed to allow insertion of a silicon probe (type I, 27 active channels separated by 50 μm, NeuroNexus Technologies; type II, 16 active channels separated by 35 μm, California Probe[6]). Signals were recorded with the Cheetah 32 channel acquisition system (Neuralynx), filtered at 0.6–6 kHz and sampled at 30 kHz. After the experiment, the mouse was euthanized with an overdose of isoflurane. The numbers of mice used for the electrophysiology experiments were 25 anaesthetized PV-ChR2 mice, 33 anaesthetized CAMKIIα-Arch mice, 25 anesthetized SOM-ChR2 mice, 9 anaesthetized VIP-ChR2 mice and 13 awake PV-ChR2 mice.

Whole-cell recordings were made with an Axopatch 700B amplifier (Axon Instruments). Patch pipettes (3–5 MΩ) were filled with internal solution containing (in mM) K-gluconate 125, KCl 5, phosphocreatine 10, MgATP 4, GTP 0.4, HEPES buffer 10 and EGTA buffer 1. Data were filtered at 2 kHz, sampled at 10 kHz and digitized by Digidata 1440 (Molecular Devices), and analysed with custom software in MATLAB (Mathworks). Recordings were made under current clamp. Step currents (duration, 2 s; amplitude, 0–1.5 nA) were injected with both laser on and off, each repeated two to four times. On the basis of the *F–I* curve (firing rate versus current amplitude; Supplementary Fig. 6), the current threshold (minimal current to evoke spiking) and the slope were determined by linear regression of the curve from the point of initial spiking.

Visual stimulation. Visual stimuli were generated with a PC computer containing a NVIDIA GeForce 6600 graphics board and presented with a XENARC 700V LCD monitor (19.7 cm × 12.1 cm, 960 × 600 pixels, 75 Hz refresh rate, 300 cd m^{-2} maximum luminance, gamma corrected with custom software) located 14 cm from the left eye, positioned such that the receptive fields of the recorded neurons were at the centre of the monitor. To determine the laminar position of each channel of the silicon probe, contrast-reversal checkerboard stimuli were presented at 2 Hz 400 times. For measuring orientation tuning and direction selectivity of V1 neurons, full-field drifting gratings (100% contrast, 2 Hz, 0.04 cycles per degree, 4 s) were presented at 24 directions (separated by 15°) in a pseudorandom sequence. After one block of 24 drifting gratings, 4 s of blank stimulus (grey screen) was presented to measure spontaneous firing rate. A total of eight blocks were presented in each experiment. To measure orientation discrimination in the behavioural experiment, drifting gratings of the same contrast and spatio–temporal frequencies (100% contrast, 2 Hz, 0.04 cycles per degree, 4 s per trial) were presented to the left eye (see below).

Optical activation and silencing. A blue laser (473 nm) combined with a yellow laser (593 nm; CrystaLaser) or a green laser (532 nm; Shanghai Laser & Optics Century Co.) was connected to an output optic fibre and turned on and off by a stimulator (Grass) under computer control. Optical activation of ChR2 was induced by blue light and optical silencing by Arch activation was induced by yellow or green light, focused on top of the craniotomy made for virus injection (for the behavioural experiment, no new craniotomy was made for optical activation). For each PV-ChR2 or CAMKIIα-Arch experiment, the laser power was adjusted manually such that, although the light caused a clear reduction in cortical firing rate, most of the recorded neurons still showed visually driven spiking responses (PV-ChR2, 0.5–1 mW of blue light, with most experiments at 0.6–0.7 mW; CAMKIIα-Arch, 2–15 mW of yellow/green light). For SOM-ChR2 and VIP-ChR2 experiments, we used blue light at powers similar to or higher than in the PV-ChR2 experiment (0.6–1.5 mW). For VIP-ChR2 experiments, increasing the laser power to 2–3 mW also did not cause strong suppression of cortical activity. For measuring changes in spontaneous firing rate induced by optical activation or silencing, 30 trials of light stimulation (5 s per trial, 25 s inter-trial interval) were applied while a blank grey screen was presented as the visual stimulus. To measure the effect of optical activation or silencing on visually evoked responses, laser stimulation began 0.5 s before the onset and ended 0.5 s after the termination of each trial of drifting grating stimulation. Because stray laser light could potentially activate the retina (either from the outside or travelling through the cortex), beginning laser stimulation before the grating stimuli helped to minimize contamination of the responses to the grating stimuli by transient spiking evoked by the onset of stray laser. We alternated between the blocks of trials (24 orientations per block) with and without laser stimulation. For the whole-cell recording experiments (Supplementary Fig. 6), laser stimulation began 200 ms before the onset of current injection and ended 800 ms after termination of the current step. For the behavioural task, laser stimulation started with the trial and lasted for 5 s, thus covering the entire duration of visual stimulation in each trial (Fig. 4b).

Data analysis. To determine the laminar position of each recording channel, multi-unit activity was aligned to the start time of the flash checkerboard stimuli and averaged across trials. Layers four and six were identified on the basis of short-onset latency of the responses. For single-unit isolation, all channels of the silicon probe were separated into groups (four channels per group), and spike waveforms were sorted using Klusters (http://klusters.sourceforge.net)[32]. To assess the quality of each sorted unit, we computed both Lratio and isolation distance[33,34]. To select high-quality single units, we set the thresholds at Lratio <0.1 and Isolation Distance >20 (a unit had to satisfy both criteria to be selected), which corresponded to a $<1\%$ error rate[34]. Among these high-quality single units, only those with firing rates greater than 0.1 spikes s^{-1} were included in further analyses. All of the analysis was performed in MATLAB.

To quantify orientation tuning and direction selectivity of each neuron, we fitted the firing rate as a function of orientation by the sum of two Gaussian functions with peaks 180° apart:

$$R(\theta)=a_0+a_1e^{\frac{-(\theta-\theta_0)^2}{2\sigma^2}}+a_2e^{\frac{-(\theta-\theta_0\pm180^0)^2}{2\sigma^2}}$$

in which $R(\theta)$ is the response at orientation θ, a_0 is the untuned component of the response, a_1 and a_2 are the amplitudes of the two Gaussians, θ_0 is the preferred orientation and σ is the standard deviation of the Gaussian function

(Supplementary Fig. 2). Tuning width is measured by σ and the DSI is measured by:

$$|a_1 - a_2|/(a_1 + a_2)$$

The fitting error was computed as:

$$E = \sum_\theta (R_{\text{measure}}(\theta) - R_{\text{fit}}(\theta))^2 / \sum_\theta (R_{\text{measure}}(\theta) - \overline{R})^2$$

in which $R_{\text{measure}}(\theta)$ and $R_{\text{fit}}(\theta)$ are the measured and fitted responses at θ, respectively, and $\overline{R}$ is the measured response averaged across all orientations. We set a threshold of 0.5 for the fitting error; σ and DSI of a cell were included in the analysis only if the fitting error was below the threshold both with and without laser stimulation.

To quantify the reliability of each measured tuning curve, we computed the signal-to-noise ratio (SNR):

$$\text{SNR} = \sum_\theta (R(\theta) - \overline{R})^2 / \sum_\theta \text{VAR}(\theta)$$

in which $R(\theta)$ is the firing rate at θ averaged across all trials, $\overline{R}$ is the mean firing rate across all orientations and VAR (θ) is the variance of the response at θ across trials.

The Pearson correlation coefficient (r) was used to quantify the relationship between the laser-induced firing-rate change and changes in tuning width and direction selectivity.

Behavioural experiment. Adult PV-ChR2 mice (P60–P100) were water-deprived for 1 day before starting the training. A total of 35 mice were used for the behavioural experiment. During daily training, the mouse was head-fixed and sat in an acrylic tube within a sound-proof training box. Tongue licks were detected by a custom-made beam-break lickometer. Training ended when the mouse seemed satiated and stopped licking for several minutes[35]. The entire behavioural experiment consisted of five phases: habituation, conditioning, easy discrimination, hard discrimination and optogenetic experiment.

For habituation (2–3 days), there was no visual stimulus and the mouse was given free water rewards (~4 µl) for each lick.

For conditioning (2–3 days), the mouse was trained to lick in response to a visual stimulus (vertically oriented grating drifting rightward; 'go stimulus'). Each trial started with a tone (0.1 s duration; 5 kHz), followed by the visual stimulus (starting 1 s after the tone; 4 s in duration) and ended with an inter-trial period of 4 s. If a lick was detected during the last 2 s of the visual stimulation (response window), the mouse was rewarded with ~4 µl of water for 2 s (hit). If no lick was detected during the response window (miss), water reward was given at the end of the visual stimulus during this conditioning phase. Once the number of hits exceeded 150 within 30 min, the mouse was advanced to the next phase.

For easy discrimination (5–10 days), each trial had the same temporal structure, but the visual stimulus was either the go or no-go (horizontally oriented grating drifting upward) stimulus. The go and no-go trials were randomly interleaved, but the same visual stimulus was never presented more than three consecutive times. Licking within the response window of a go trial (hit) was rewarded with water, whereas licking in the response window of a no-go trial (FA) was punished with a mild air puff (100 ms) and a longer inter-trial interval (8 s, timeout). The mouse was neither rewarded nor punished for a miss (no-lick in a no trial) or correct rejection (CR, no-lick in a no-go trial). Hit and FA rates were quantified as follows:
Hit rate = number of hits/(number of hits + number of misses) and
FA rate = number of FAs/(number of FAs + number of CRs). On the basis of the hit and FA rates, d' was quantified by: d' = norminv(hit rate) – norminv(FA rate) in which norminv is the inverse of the cumulative normal function[20,36]. Higher d' values indicate better performance in visual discrimination.

If a threshold performance ($d' > 1$) was reached within 10 days for the easy discrimination task (orientation difference between go and no-go stimuli, $\Delta\theta = 90^\circ$), the mouse was advanced to the next phase. Some of the mice failed to reach the threshold, and they were not further tested.

For hard discrimination (>5 days), each test block consisted of 20 trials, in which go and no-go trials at a fixed $\Delta\theta$ were randomly interleaved ($\Delta\theta = 30^\circ, 60^\circ$ or 90°). To ensure that the mouse stayed motivated, we alternated between a 'relearning' block ($\Delta\theta = 90^\circ$) and a 'test' block ($\Delta\theta = 30^\circ, 60^\circ$ or 90°; the sequence among test blocks of different $\Delta\theta$ was pseudorandom). For each mouse, the orientation of either go or no-go stimulus was fixed, whereas $\Delta\theta$ changed across blocks. d' was then measured as a function of $\Delta\theta$. When $d' > 0.5$ for $\Delta\theta = 30^\circ$, we added test blocks with $\Delta\theta = 10^\circ$ (that is, we alternated between the relearning block with $\Delta\theta = 90^\circ$ and a test block with $\Delta\theta = 10^\circ, 30^\circ, 60^\circ$ or 90°). The addition of this most difficult block ($\Delta\theta = 10^\circ$) often caused a considerable drop in the overall performance, probably caused by a loss of motivation owing to the high failure rate. We continued the training in this phase until the performance recovered to a level comparable to that before adding the block with $\Delta\theta = 10^\circ$.

For the optogenetic experiment, the effect of optical activation of PV^+ neurons on orientation discrimination was measured at $\Delta\theta = 10^\circ, 30^\circ, 60^\circ$ and 90°. In each block, laser stimulation was applied in 50% of randomly selected trials, and d' was analysed separately for trials with and without laser stimulation. To eliminate the trials near the end of each session, when the mouse was satiated and lost motivation for the task, we only included the trials with >50% hit rate within 100 consecutive trials. To minimize the amount of laser light reaching the eyes, the optic fibre was shielded by a black tape.

Because very strong suppression of visually driven cortical responses can negatively affect perception, the laser power was chosen carefully to match between the behavioural and electrophysiological experiments. We first measured the loss of laser power through the skull (craniotomy was made for the acute electrophysiological experiments but not for the chronic behavioural experiments) *in vitro* by passing the laser beam through the skull of a mouse previously used in the behaviour experiment (note that a small hole was drilled during virus injection several weeks before the behavioural experiment, so the skull at the injection site is thinner than at other places; our calibration was performed at the injection site). We found ~30% loss of power after passing through the skull. Because in most of the PV-ChR2 electrophysiology experiments we used 0.6–0.7 mW of laser power, which was found to be effective in sharpening the tuning curve without excessive suppression of cortical activity, we chose 0.8–1 mW laser power for the behavioural experiments. Each mouse was tested in up to eight sessions (one session per day), and all animals tested with the 0.8–1 mW laser were included ($n = 25$).

Among the 25 PV-ChR2 mice tested, 6 were advanced directly from easy discrimination to optogenetic experiment, and the effect of PV activation was tested only at $\Delta\theta = 90^\circ$; 10 mice were trained in hard discrimination at $\Delta\theta = 30^\circ, 60^\circ$ and 90° and the effect of laser was tested at these three angles; the remaining 9 mice were trained in hard discrimination at $\Delta\theta = 10^\circ, 30^\circ, 60^\circ$ and 90° before the effect of laser was tested at all four angles.

31. Maheshri, N. *et al.* Directed evolution of adeno-associated virus yields enhanced gene delivery vectors. *Nature Biotechnol.* **24,** 198–204 (2006).
32. Hazan, L. *et al.* Klusters, NeuroScope, NDManager: a free software suite for neurophysiological data processing and visualization. *J. Neurosci. Methods* **155,** 207–216 (2006).
33. Harris, K. D. *et al.* Accuracy of tetrode spike separation as determined by simultaneous intracellular and extracellular measurements. *J. Neurophysiol.* **84,** 401–414 (2000).
34. Schmitzer-Torbert, N. *et al.* Quantitative measures of cluster quality for use in extracellular recordings. *Neuroscience* **131,** 1–11 (2005).
35. O'Connor, D. H. *et al.* Vibrissa-based object localization in head-fixed mice. *J. Neurosci.* **30,** 1947–1967 (2010).
36. Green, D. M. & Swets, J. A. *Signal Detection Theory and Psychophysics* (Wiley, 1966).

doi:10.1038/nature11312

Supplementary Figures and Legends

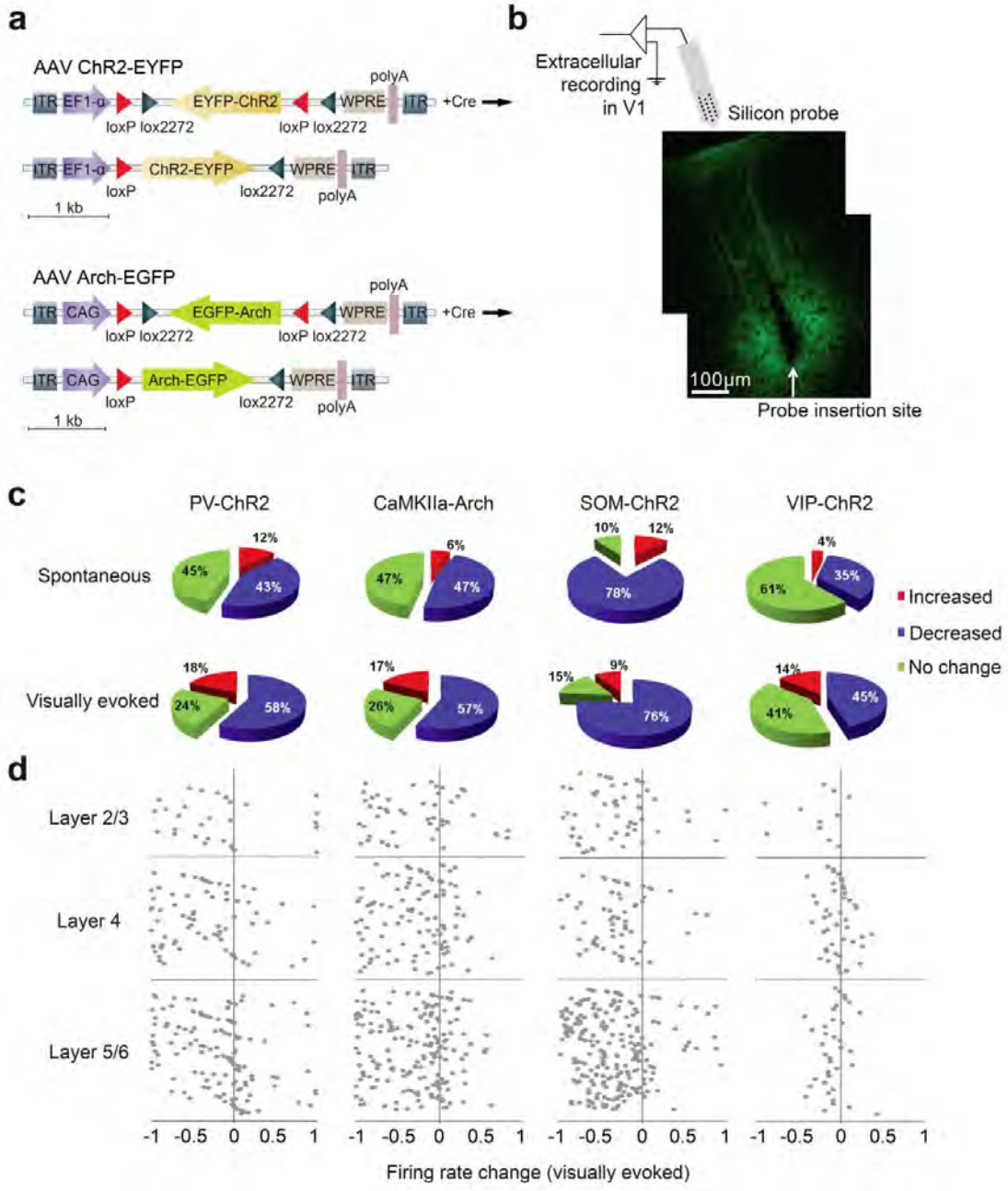

Supplementary Figure 1 | Changes in firing rate induced by laser stimulation in different cortical layers in anesthetized mouse V1. **a,** Schematics for the viral vectors used for cell-type specific expression of ChR2 and Arch. **b**, Fluorescence image showing the insertion site of the silicon probe in V1 injected with the viral vector. Image was from a CaMKIIα-ChR2-EYFP mouse. **c**, Fractions of neurons showing significant increase ($P < 0.01$, bootstrap), significant decrease, and no significant change in spontaneous (upper row) and

visually evoked (lower row) firing rates upon laser stimulation, in PV-ChR2, CaMKIIα-Arch, SOM-ChR2, and VIP-ChR2 mice. **d**, Changes in visually evoked firing rate in different cortical layers induced by ChR2-mediated activation of different types of inhibitory interneurons or Arch-mediated silencing of excitatory neurons, measured by $(R_{light\text{-}on} - R_{light\text{-}off})/(R_{light\text{-}on} + R_{light\text{-}off})$, where $R_{light\text{-}on}$ and $R_{light\text{-}off}$ are firing rates during laser on and off periods, respectively, averaged across all orientations. Each symbol represents one single unit. The layers were identified based on the recording depth (layer 2/3, 100 μm - 350 μm; layer 4, 350 μm - 500 μm; layer 5/6, 500 μm - 1 mm) as well as multiunit activity in response to a transient visual stimulus (layers 4 and 6 showed short latencies of 40 to 50 ms, and layer 2/3 and 5 showed delayed responses at 70 to 100 ms).

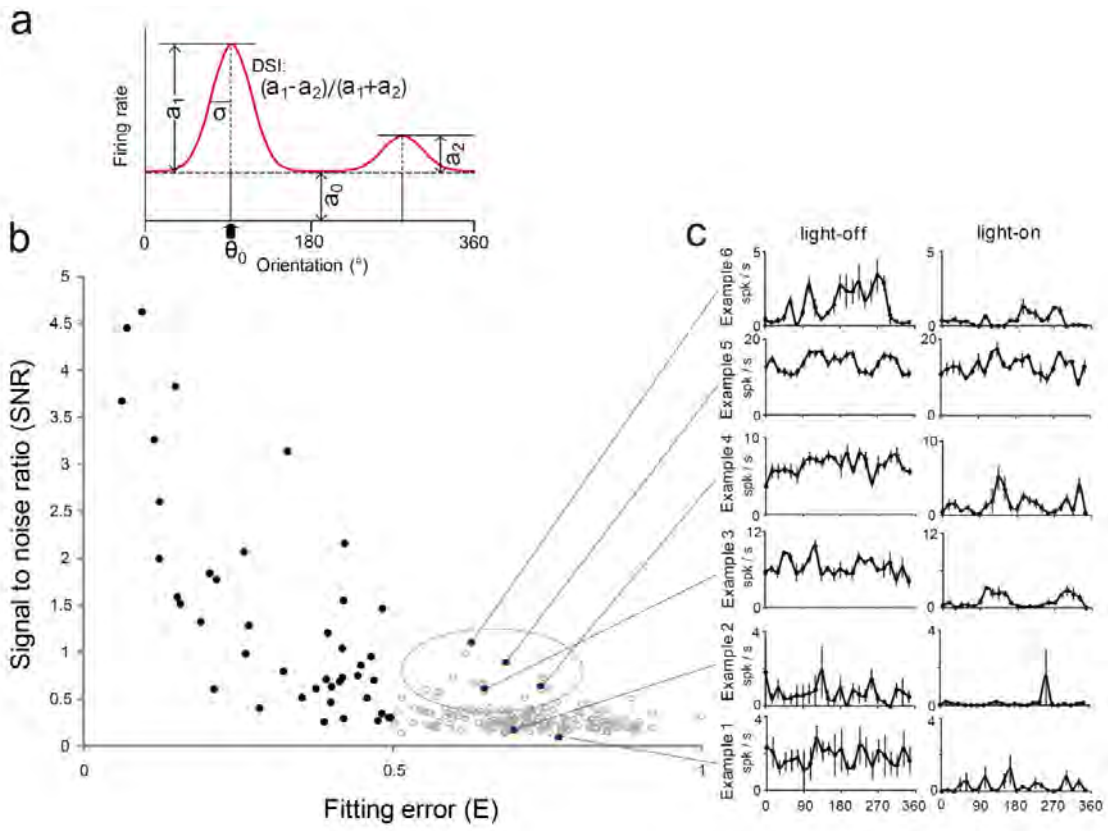

Supplementary Figure 2 | Quantification of orientation tuning and direction selectivity by fitting with a double Gaussian function. **a**, Schematic illustration of the parameters of the double Gaussian function. **b**, Scatter plot of signal-to-noise ratio (SNR) of the tuning curve vs. fitting error (E) in the PV-ChR2 group. Each symbol represents one cell. Black filled dots, cells with E < 0.5, included in the quantitative analysis of σ and DSI. Gray open circles, cells with E > 0.5, excluded from the quantitative analysis. Blue filled dots, cells whose tuning curves are shown in **c**. Dotted ellipse, cells with E > 0.5, but relatively high SNR. **c**. Six example cells (blue filled dots in **b**).

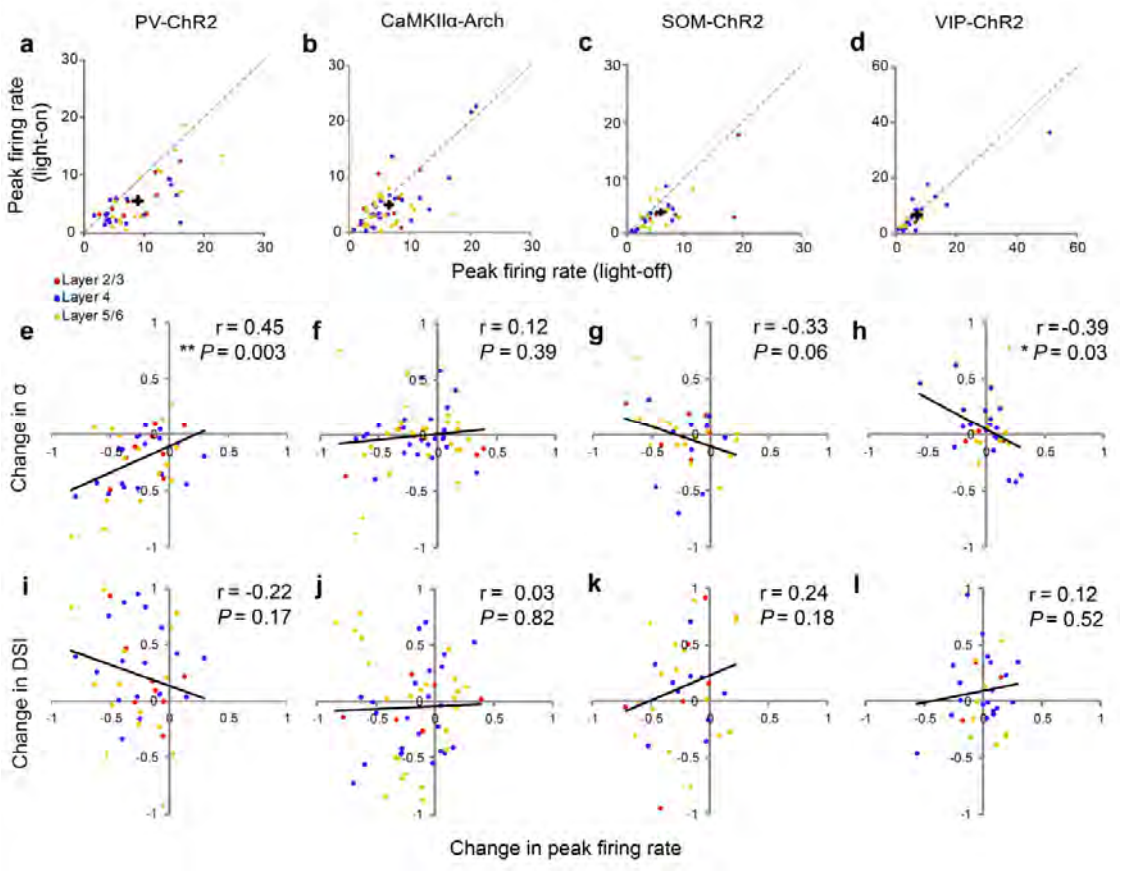

Supplementary Figure 3 | Laser-induced changes in peak firing rate and stimulus selectivity measured in PV-ChR2, CaMKIIα-Arch, SOM-ChR2, and VIP-ChR2 mice. a-d, peak firing rate (firing rate at the preferred orientation and direction) with laser on vs. laser off. Each dot represents one cell. Layers are represented by colors. Cross, population average (± s.e.m.). **e-h**, Change in σ (measured by $(\sigma_{light\text{-}on} - \sigma_{light\text{-}off})/(\sigma_{light\text{-}on} + \sigma_{light\text{-}off})$) vs. peak firing rate change. **i-l**, Change in DSI (measured by $(DSI_{light\text{-}on} - DSI_{light\text{-}off})/(DSI_{light\text{-}on} + DSI_{light\text{-}off})$) vs. peak firing rate change. Circle, individual cell. Line, linear regression for the population.

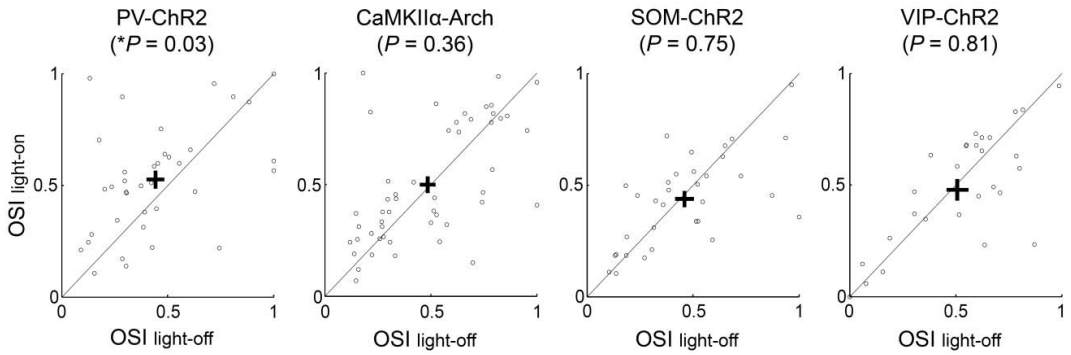

Supplementary Figure 4 | Laser-induced changes in orientation selectivity index in PV-ChR2, CaMKIIα-Arch, SOM-ChR2, and VIP-ChR2 mice. Orientation selectivity index (OSI) was calculated as 1 - circular variance[23]. Laser stimulation caused a significant increase in OSI in PV-ChR2 mice but not in CaMKIIα-Arch, SOM-ChR2, or VIP-ChR2 mice (paired *t*-test).

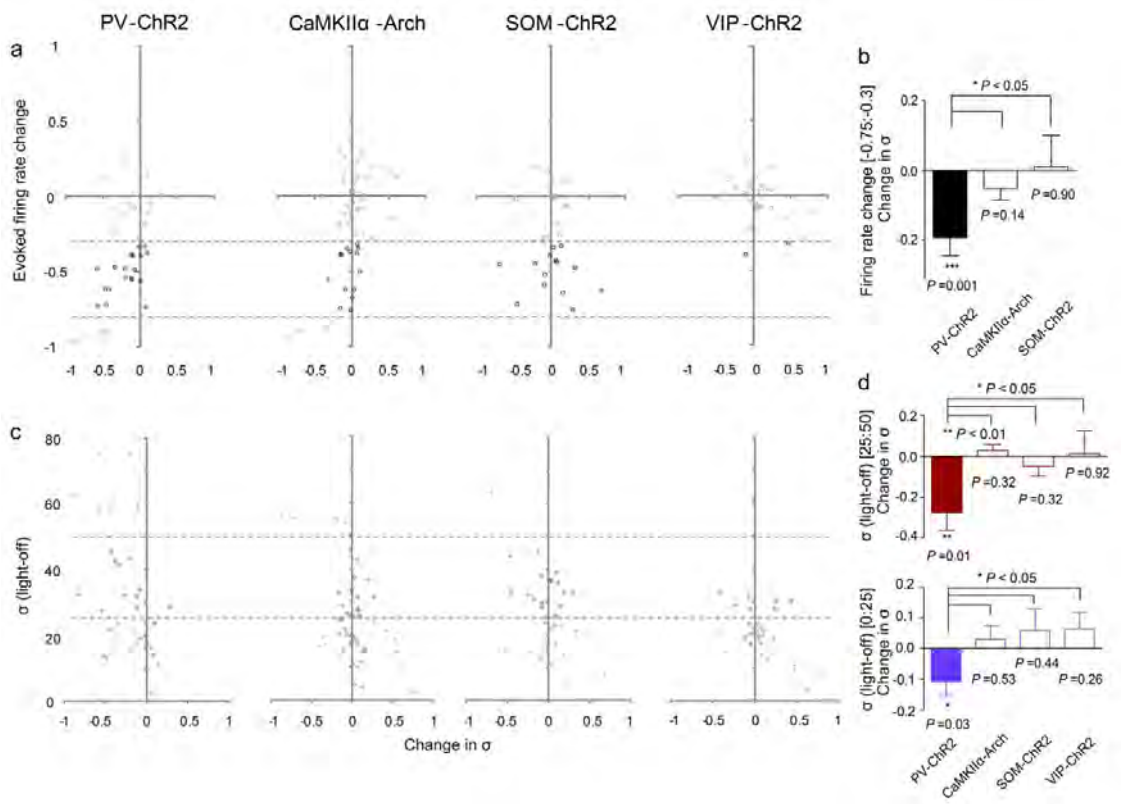

Supplementary Figure 5 | Comparison of laser-induced changes in σ across groups with matching firing rate change and σ (light-off). **a**, Scatter plot of evoked firing rate change (laser induced change in visually evoked firing rate, averaged across all orientations) vs. change in σ, for the four groups of cells. Each symbol represents one cell. Dashed lines delineate the range of firing rate change [-0.75 -0.3] within which the four groups were compared. Note that except for the VIP-ChR2 group, the firing rate change was well matched among the other three groups within this range. **b**, Laser-induced change in σ for cells within the range indicated in **a** in each group, mean ± s.e.m. The VIP-ChR2 group was omitted since there were only two cells in the range. The reduction was significant in the PV-ChR2 (solid bar) but not in CaMKIIα-Arch and SOM-ChR2 groups (open bars), *P* value below each bar indicates significance of the change within each group. The difference between the PV-ChR2 and each of the other two groups was significant (*P* value on top of plot). **c**, Scatter plot of σ (light-off) vs. change in σ, for the four groups of cells. Dashed lines delineate the two ranges of σ (light-off), broad ([25° 50°], red) and narrow ([0° 25°], blue), within which the four groups were compared. **d**, Laser-induced change in σ for cells within the broad (upper) and narrow (lower) ranges in each group, mean ± s.e.m. The reduction was significant in the PV-ChR2 (solid bar) but not in the CaMKIIα-Arch, SOM-ChR2 and VIP-ChR2 (open bar) groups, and the difference between PV-ChR2 and each of the other three groups was significant.

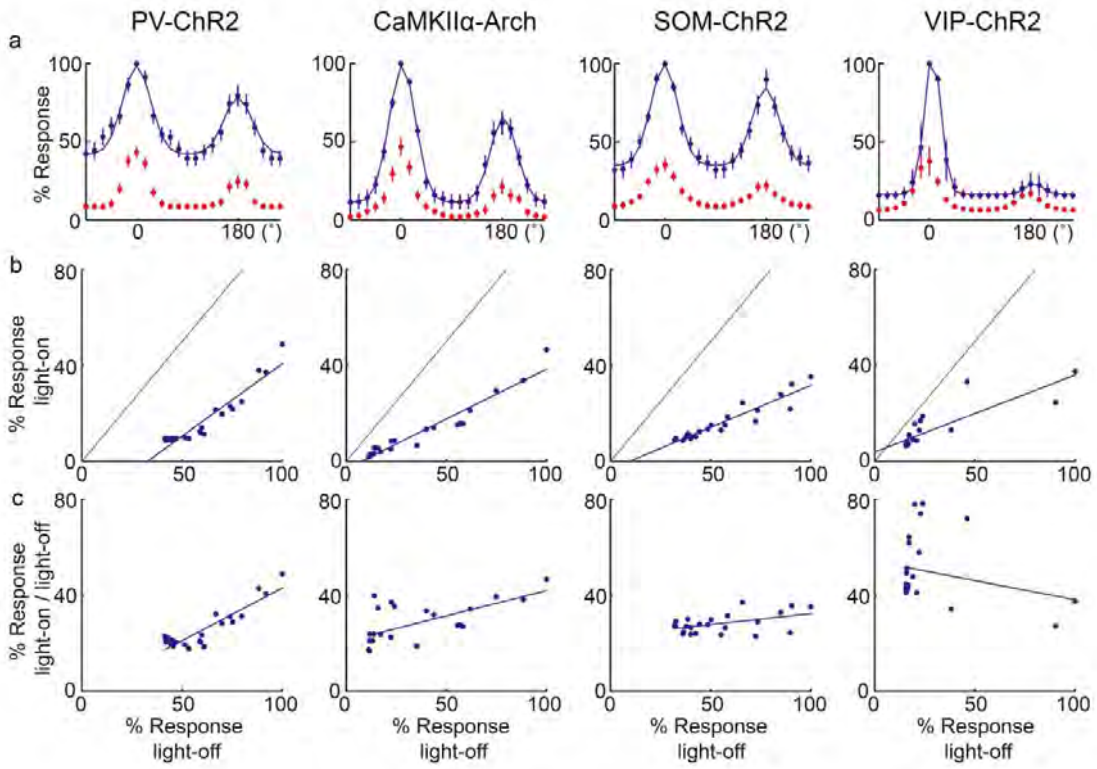

Supplementary Figure 6 | Effects of laser on firing rates at different stimulus directions for neurons in PV-ChR2, CaMKIIα-Arch, SOM-ChR2 and VIP-ChR2 groups whose firing rate changes fall between -0.75 and -0.3 (between dashed lines in Supplementary Fig. 5a). a, Median response of the neurons to 24 directions with (red) or without (blue) laser stimulation. The median response was computed after aligning the tuning curves of all cells in each group to the same preferred orientation (0°). Blue line: fit with double Gaussian function to the response without laser stimulation. **b**, Median responses to 24 directions with laser stimulation plotted against those without laser. Line, linear fit to data (PV-ChR2, slope 0.61, horizontal offset 32.7%; CaMKIIα-Arch, slope 0.42, offset 7.6%; SOM-ChR2, slope 0.35, offset 9.5%; VIP-ChR2, slope 0.32, offset -12.1%). The plots in **a** and **b** are analogous to Fig. 4A,B in the study of Atallah et al[23]. **c**, Amount of laser-induced suppression vs. response without laser at each stimulus direction. Line, linear fit to data (slope: PV-ChR2, 0.44; CaMKIIα-Arch, 0.21; SOM-ChR2, 0.09; VIP-ChR2, -0.16). Note that among the four groups PV-ChR2 shows the strongest correlation between the degree of suppression and the response without laser. Stronger suppression of the responses at non-preferred orientations caused sharpening of tuning.

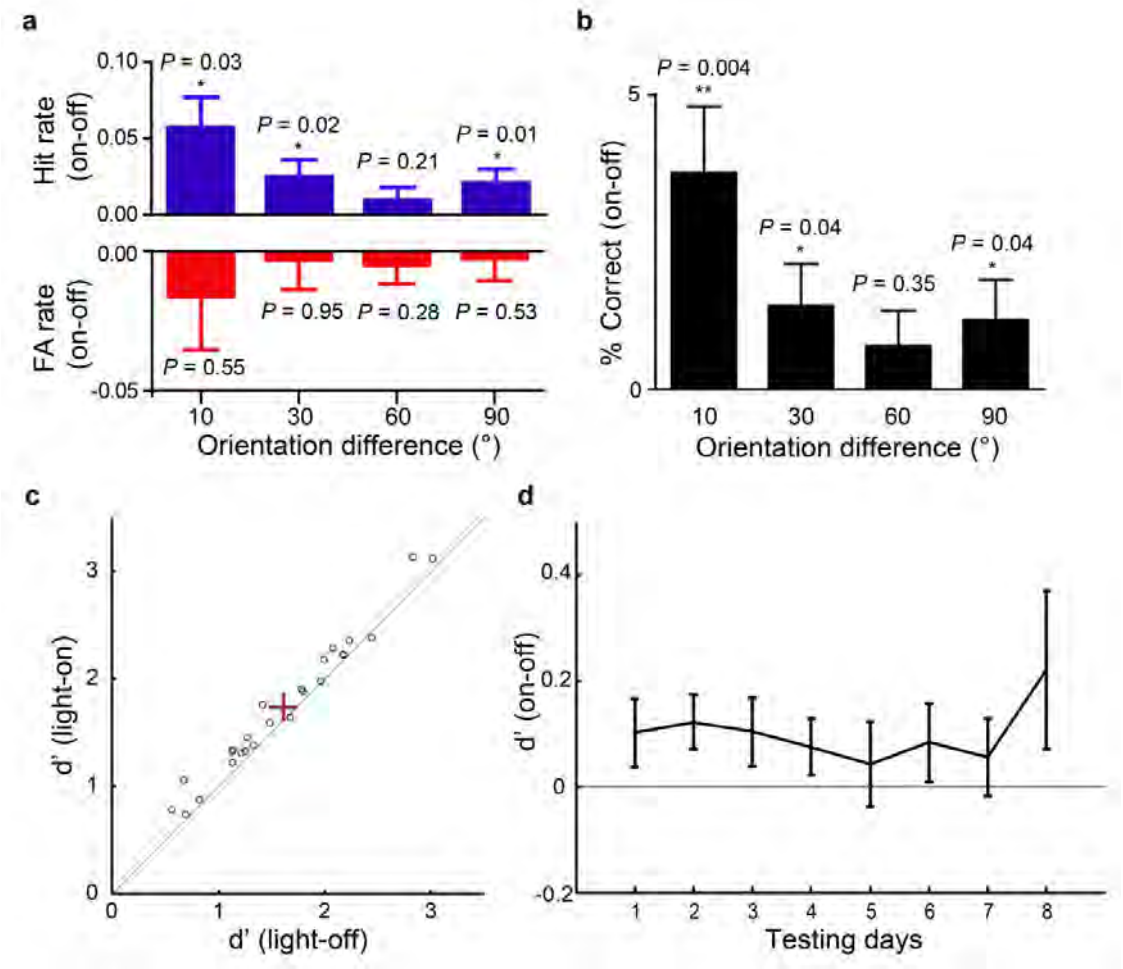

Supplementary Figure 7 | Effects of PV+ neuron activation on orientation discrimination. **a**, Effect of laser on hit and false alarm rates at each of the four Δθ values, measured by the difference between the laser on and laser off trials for each mouse, averaged across all mice (n = 9 to 25). Error bar, ± s.e.m. *P* value on top of each bar indicates significance of the effect of laser stimulation at each orientation difference. **b**, Laser-induced change in % of correct trials. **c**, d' of each mouse (combined across all Δθ values and all test sessions) during laser on vs. laser off. The difference between light-on and light-off was significant ($P = 4 \times 10^{-5}$, Wilcoxon signed rank test, n = 25). **d**, Effect of laser stimulation on d' over multiple days of testing. For each mouse the data at all Δθ values were combined. Error bar, ± s.e.m.

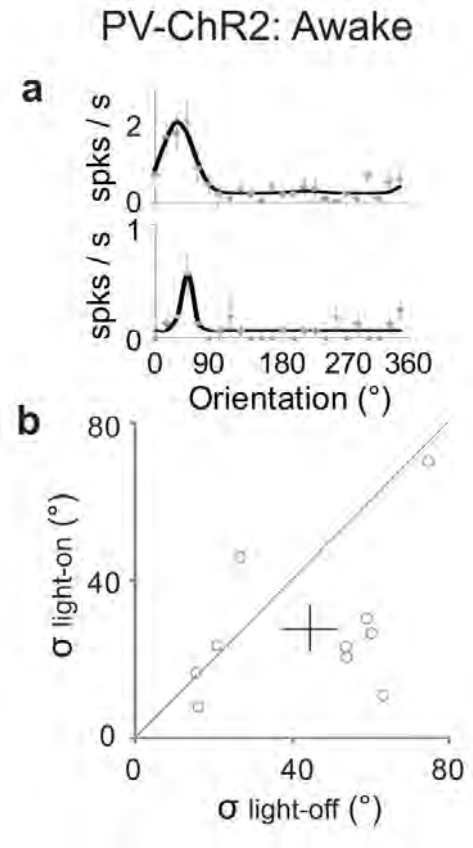

Supplementary Figure 8 | Effect of laser stimulation on orientation tuning in awake PV-ChR2 mice. **a**, Example tuning curves. **b,** σ with and without laser stimulation (light-off, 44.2 ± 7.0^{o}, light-on, 27.9 ± 5.8^{o}, mean ± s.e.m., n = 10; $P < 0.05$, paired *t*-test).